Design and Implementation of Bidirectional DC-DC CLLLC Resonant Converter

Hao-Tang Chang, Tsorng-Juu Liang, *Fellow, IEEE*, Wei-Chin Yang
Department of Electrical Engineering
Hierarchical Green-Energy Materials Research Center/Green Energy Electronics Research Center (GREERC)
National Cheng-Kung University, Tainan, Taiwan
Email: tjliang@mail.ncku.edu.tw

***Abstract*—An isolated bidirectional resonant converter with digital control is presented in this paper for the energy transferring between the DC bus and the EV battery. The main circuit topology consists of full-bridge structures and a CLLLC resonant tank. Due to the bidirectional symmetrical characteristics of the circuit, the complexity of the bidirectional power flow control can be reduced. This converter can also achieve soft switching to improve the efficiency. A laboratory prototype converter with rated power 4.4 kW, DC bus voltage 400 V and battery voltage 200~410 V is implemented to validate the theoretical analysis. During the bidirectional operation, the maximum conversion efficiency is 96.5 %.**

Keywords—bidirectional power flow, DC-DC power converter, zero voltage switching, battery chargers

I. Introduction

In recent years, electric vehicles (EVs) have gained more acceptance on the market. These vehicles reduce not only the petroleum consumption but also air pollution and noise, but there still have some concerns compared with fuel vehicles. Therefore, the developments of EV battery chargers are eventually received attention [1]. Because of the V2G concept [2], some EV battery chargers can be operated in bidirectional power flow. Isolated bidirectional DC-DC converters are used to control the power flow between the DC bus and the battery and provide galvanic isolation. To achieve compact size and high efficiency, high switching frequency and soft-switching technique are necessary, thus, the advanced researches in the isolated bidirectional DC-DC converters are developed [3]-[13]. Recently, the soft-switching resonant converters [10]-[15] are attractive topologies to improve the efficiency.

In this paper, the operational principles, voltage-gain characteristics, and design procedure of the bidirectional DC-DC CLLLC resonant converter applied in the EV battery chargers are analyzed and discussed. With the resonant manner, the ZVS on the switches and the ZCS on the rectifiers can be achieved without an additional circuit. Furthermore, to achieve more functions and simplify the control circuit, the converter is implemented with a digital signal processor (DSP). A 4.4 kW prototype converter is implemented and tested in bidirectional power conversion.

II. Ananlysis of Bidirectional CLLLC Resonant Converter

Fig. 1 shows the circuit topology and the voltage-gain curves of the bidirectional resonant converter. This topology consists of the symmetric full-bridge structures and the CLLLC-type resonant tank so the function of transferring

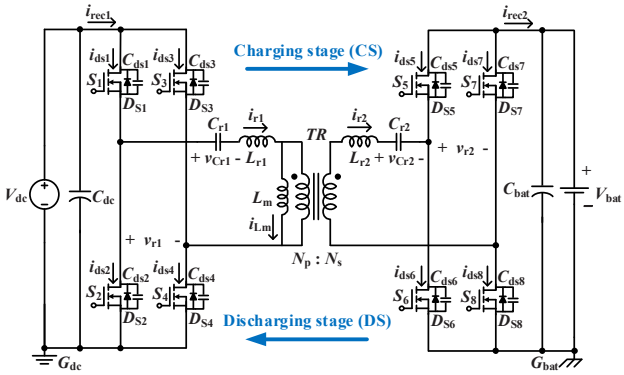

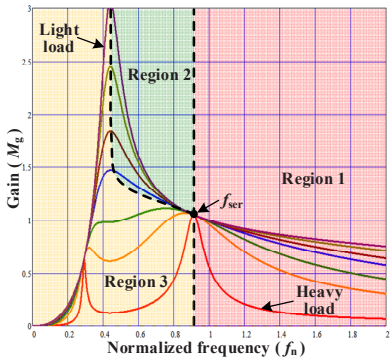

Fig. 1. Topology and voltage-gain curves of bidirectional DC-DC CLLLC resonant converter.

power in either direction can be easily achieved. The characteristics of this topology are similar to the conventional LLC resonant converter with extra resonant components (L_{r2} and C_{r2}) in the secondary side.

Due to the CLLLC-type resonant tank, the voltage-gain curves of the bidirectional resonant converter have three resonant frequencies which are composed of different resonant components based on the load conditions. For the purposes of the monotonic voltage-gain curves and the inductive impedance of the resonant tank, the converter is defined to be operated in region 1 and region 2.

The key waveforms of the bidirectional DC-DC CLLLC resonant converter operating above resonant frequency are shown in Fig. 2. In this operating condition, the controlled switches can achieve ZVS turn-on, but the output rectifier is hard-switching. The operating modes from t_5 to t_{10} are symmetrical to those of the previous half cycle, so these modes are omitted in this section.

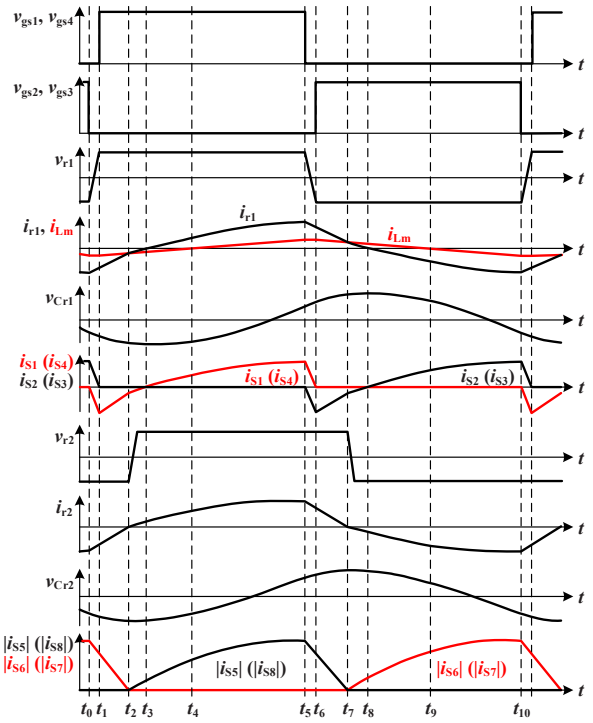

Fig. 2. Operational principles of bidirectional DC-DC CLLLC resonant converter above resonant frequency.

Mode I [t_0-t_1]: At t = t_0, the gate signals v_{gs2} and v_{gs3} change to low level. The resonant current ir1 discharges the output capacitors of S_1 and S_4, and charges the output capacitors of S_2 and S_3. The current difference between i_{r1} and i_{Lm} is transferred to the battery side. This mode ends when C_{ds1} and C_{ds4} are fully discharged and C_{ds2} and C_{ds3} are fully charged. Then, the anti-parallel diodes of S_1 and S_4 conduct, which makes the switches achieve ZVS turn-on. The gate signals v_{gs1} and v_{gs4} change to high level.

Mode II [t_1-t_2]: At $t = t_1$, the switches S_1 and S_4 are turned on with ZVS. The DC bus voltage V_{dc} forces the slope of i_{r1} and i_{Lm} to change from negative to positive. The magnetizing inductor L_m does not participate in the resonance during this mode so the magnetizing current i_{Lm} increases linearly. Since i_{r1} is less than i_{Lm}, the DC bus side energy can be transferred to the battery side rectifier through the transformer *TR* and provided to load through D_{S6} and D_{S7}. This mode ends when the resonant current i_{r1} reaches i_{Lm}.

Mode III [t_2-t_3]: At $t = t_2$, the current i_{r2} changes to positive direction since i_{r1} is greater than i_{Lm}. Because L_m also does not participate in the resonance during this mode, i_{Lm} still increases linearly. Besides, the resonant capacitor C_{r1} is charged by i_{r1}, which makes the slope of v_{Cr1} increase gradually. The DC bus side energy is transferred to the battery side rectifier through *TR* and then provided to load through D_{S5} and D_{S8}. This mode ends when i_{r1} increases to zero.

Mode IV [t_3-t_4]: At $t = t_3$, the resonant current i_{r1} changes from negative to positive direction. The current difference between i_{r1} and i_{Lm} will be transferred to the battery side. Since the current difference between i_{r1} and i_{Lm} is increasing, the current i_{r2} also increases gradually. The DC bus side energy is continuously transferred to the battery side rectifier through the transformer *TR* and provided to load through D_{S5} and D_{S8}. This mode ends when i_{Lm} increases to zero.

Mode V [t_4-t_5]: At $t = t_4$, i_{Lm} changes to positive direction, and the current difference between i_{r1} and i_{Lm} increases so the current i_{r2} keeps increasing. During this mode, L_m does not participate in the resonant operation. Thus, i_{Lm} still increases linearly. The DC bus side energy is continuously transferred to the load. Since the energy from the DC bus side is larger than the load requirement, the filter capacitor C_{bat} is charged during this mode. This mode ends when the gate signals v_{gs1} and v_{gs4} change to low level. At $t = t_5$, the current i_{r2} increases to the maximum value.

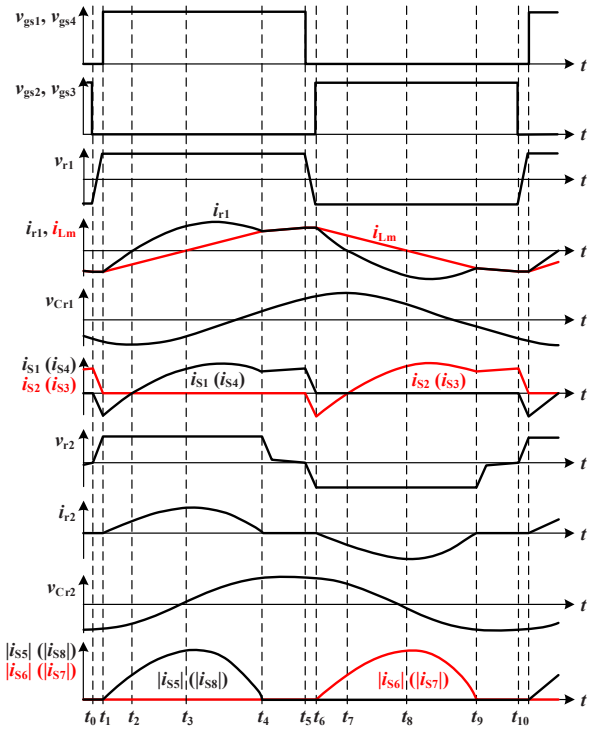

Fig. 3. Operational principles of bidirectional DC-DC CLLLC resonant converter below resonant frequency.

The key waveforms of the bidirectional DC-DC CLLLC resonant converter operating below resonant frequency are shown in Fig. 3. In this operating condition, the controlled switches can achieve ZVS turn-on, and the output rectifier can achieve ZCS turn-off. The operating modes from t_5 to t_{10} are symmetrical to those of the previous half cycle, so these modes are omitted in this section.

Mode I [t_0-t_1]: At t = t_0, the gate signals v_{gs2} and v_{gs3} change to low level. The resonant current ir1 discharges the output capacitors of S_1 and S_4, and charges the output capacitors of S_2 and S_3. The current difference between i_{r1} and i_{Lm} is transferred to the battery side. This mode ends when C_{ds1} and C_{ds4} are fully discharged and C_{ds2} and C_{ds3} are fully charged. Then, the anti-parallel diodes of S_1 and S_4 conduct, which makes the switches achieve ZVS turn-on. The gate signals v_{gs1} and v_{gs4} change to high level.

Mode II [t_1-t_2]: At $t = t_1$, the switches S_1 and S_4 are turned on with ZVS. The DC bus voltage V_{dc} forces the slope of i_{r1} and i_{Lm} to change from negative to positive. The magnetizing inductor L_m does not participate in the resonance during this mode so the magnetizing current i_{Lm} increases linearly. Since i_{r1} is less than i_{Lm}, the DC bus side energy can be transferred to the battery side rectifier through the transformer *TR* and

provided to load through D_{S6} and D_{S7}. This mode ends when the resonant current i_{r1} reaches i_{Lm}.

Mode III [t_2-t_3]: At $t = t_2$, the current i_{r2} changes to positive direction since i_{r1} is greater than i_{Lm}. Because L_m also does not participate in the resonance during this mode, i_{Lm} still increases linearly. Besides, the resonant capacitor C_{r1} is charged by i_{r1}, which makes the slope of v_{Cr1} increase gradually. The DC bus side energy is transferred to the battery side rectifier through *TR* and then provided to load through D_{S5} and D_{S8}. This mode ends when i_{r1} increases to zero.

Mode IV [t_3-t_4]: At $t = t_3$, the resonant current i_{r1} changes from negative to positive direction. The current difference between i_{r1} and i_{Lm} will be transferred to the battery side. Since the current difference between i_{r1} and i_{Lm} is increasing, the current i_{r2} also increases gradually. The DC bus side energy is continuously transferred to the battery side rectifier through the transformer *TR* and provided to load through D_{S5} and D_{S8}. This mode ends when i_{Lm} increases to zero.

Mode V [t_4-t_5]: At $t = t_4$, i_{Lm} changes to positive direction, and the current difference between i_{r1} and i_{Lm} increases so the current i_{r2} keeps increasing. During this mode, L_m does not participate in the resonant operation. Thus, i_{Lm} still increases linearly. The DC bus side energy is continuously transferred to the load. Since the energy from the DC bus side is larger than the load requirement, the filter capacitor C_{bat} is charged during this mode. This mode ends when the gate signals v_{gs1} and v_{gs4} change to low level. At $t = t_5$, the current i_{r2} increases to the maximum value.

Based on the fundamental harmonic approximation (FHA) approach, the steady-state models are obtained as shown in Fig. 4, which refer all the resonant components from the load side to the source side. The structures of the resonant tank in both stages are symmetrical, but the value of

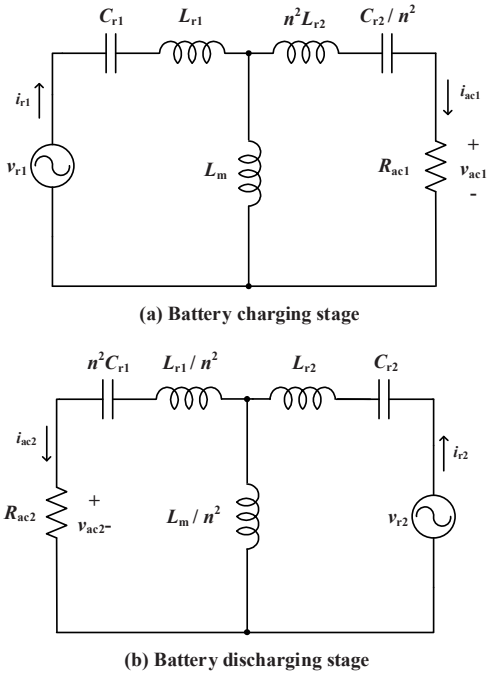

Fig. 4. FHA models of bidirectional DC-DC CLLLC resonant converter.

equivalent circuit components are different resulting in different voltage-gain characteristics in each direction.

According to the FHA models, the voltage-gain functions of the resonant tank from input to output are obtained. By substituting the impedance of the resonant components and the defined parameters, the simplified voltage-gain functions in both stages with considering the turns-ratio of the transformer can be expressed as

$$M_{CS,t} = \frac{k}{n\left|\frac{Q_{CS}}{m}\left[-m(2k+1)f_n + (k+1)(m+1)f_n^{-1} - f_n^{-3}\right] + j(k+1-f_n^{-2})\right|} \quad (1)$$

$$M_{DS,t} = \frac{nk}{\left|Q_{DS}\left[-(2k+1)f_n + (k+1)(m+1)f_n^{-1} - mf_n^{-3}\right] + j(k+1-f_n^{-2})\right|} \quad (2)$$

In addition, f_n is the normalized frequency, Q is the defined quality factor, k is the inductance ratio, and m is the capacitance ratio. Some definitions and assumptions of the resonant tank are given by

$$f_{ri} = \frac{1}{2\pi\sqrt{L_{ri}C_{ri}}},\ f_n = \frac{f_s}{f_{ri}},\ Q = \frac{\sqrt{L_{ri}/C_{ri}}}{R_{aci}},\ k = \frac{L_m}{L_{r1}},\ m = \frac{C_{r2}/n^2}{C_{r1}},\ L_{r1} = n^2L_{r2} \quad (3)$$

Where R_{ac} is the AC equivalent resistance, and i is equal to 1 in CS and 2 in DS. Since the series resonant frequency in both stages is composed of the same resonant components, the series resonant frequency can be expressed as

$$f_{ser} = \frac{1}{2\pi\sqrt{(L_{r1}+n^2L_{r2})\left(\frac{C_{r1}C_{r2}/n^2}{C_{r1}+C_{r2}/n^2}\right)}} = \sqrt{\frac{m+1}{2m}}f_{r1} = \sqrt{\frac{m+1}{2}}f_{r2} \quad (4)$$

The voltage-gain curves behave as a function of four factors, including f_n, Q, k and m. After the circuit design is complete, f_n is the controlled variable and the parameters Q, k and m are constant value. However, during the design procedure, these parameters are the key factors which will affect the performance of the converter.

III. Design Methodology of Bidirectional CLLLC Resonant Converter

During the design procedure, some key points should be noticed that the voltage-gain curves should keep monotonic within the acceptable range of operating frequency and meet the voltage-gain requirements at all load and line conditions in both stages. Besides, the ZVS conditions should be achieved, and high operating frequency is required to reduce the size and cost of the circuit. The design procedure is listed by the following steps:

1) Design of the turns-ratio of transformer (n): While the converter is operated at the series resonant frequency, the maximum efficiency is obtained because low circulating energy, ZVS and ZCS conditions can be achieved. Therefore, the turns-ratio of the transformer is calculated by the nominal battery voltage and the DC bus voltage as

$$n = \frac{N_p}{N_s} = \frac{V_{bus}}{V_{bat,nom}} \quad (5)$$

2) Design of the magnetizing inductance (L_m): To ensure the output capacitor of the switches can be totally charged and discharged, the large enough resonant current and dead-

time are required. However, the magnitude of the resonant current depends on the magnetizing inductance so the maximum magnetizing inductance is expressed as

$$L_{\mathrm{m}} \le \frac{t_{\mathrm{d}} T_{\mathrm{s}}}{8 C_{\mathrm{oss}}} \tag{6}$$

3) Design of the quality factors (Q_{CS} and Q_{DS}): Because of the defined parameters previously, there is a relationship that the range of Q_{DS} will vary with Q_{CS}. As shown in Fig. 5, while the quality factors increase, the voltage gain will decrease and lose monotonicity. Therefore, the maximum quality factors should be determined chiefly to keep the

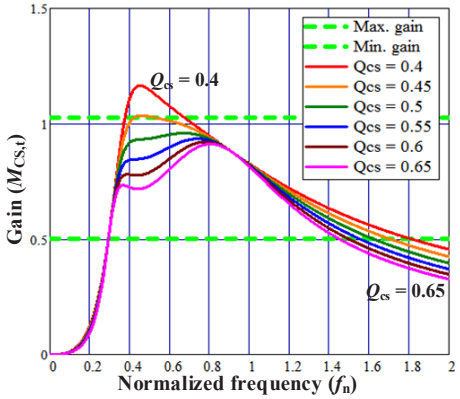

(a) Battery charging stage

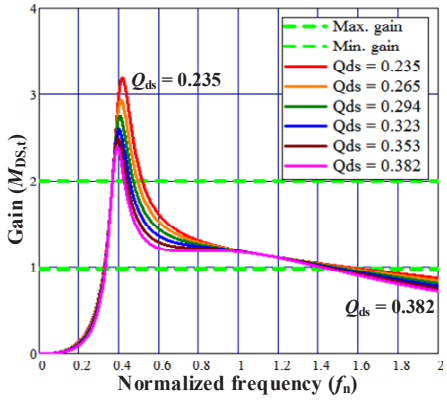

(b) Battery discharging stage

Fig. 5. Voltage-gain curves with different value of Q.

circuit operated within the inductive region.

4) Design of the inductance ratio (k): As shown in Fig. 6, the RMS resonant current in both stages decreases when the value of k increases. As the value of k increases, the RMS resonant current gradually approaches to a steady value. As shown in Fig. 7, the large value of k will also decrease the voltage gain and make the range of operating frequency becomes wide

5) Design of the capacitance ratio (m): As shown in Fig. 8, when the value of m increases, the voltage gain increases in CS but decreases in DS. The resonant capacitance cannot be too large, as this will decrease the impedance of the resonant tank which requires high switching frequency to limit the start-up resonant current.

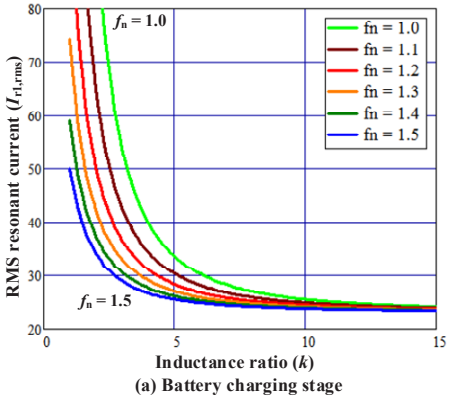

(a) Battery charging stage

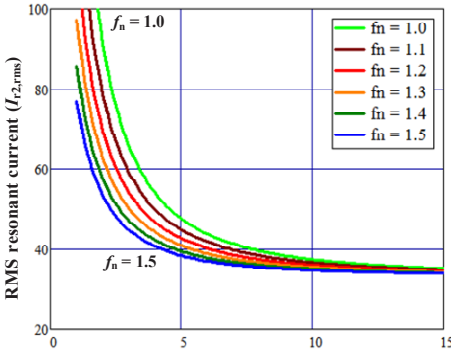

(b) Battery discharging stage

Fig. 6. RMS resonant current with different value of k and f_n.

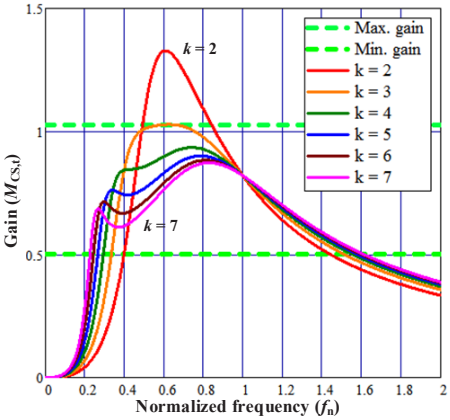

(a) Battery charging stage

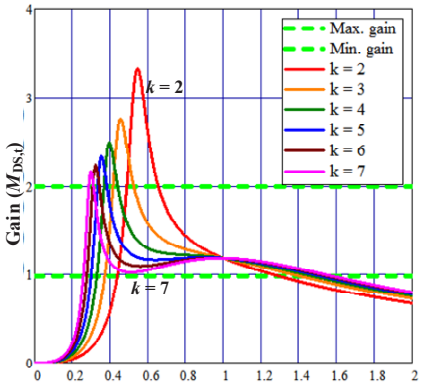

(b) Battery discharging stage

Fig. 7. Voltage-gain curves with different values of k.

6) Calculation of the resonant components: After the parameters are designed, the resonant components can be calculated, respectively.

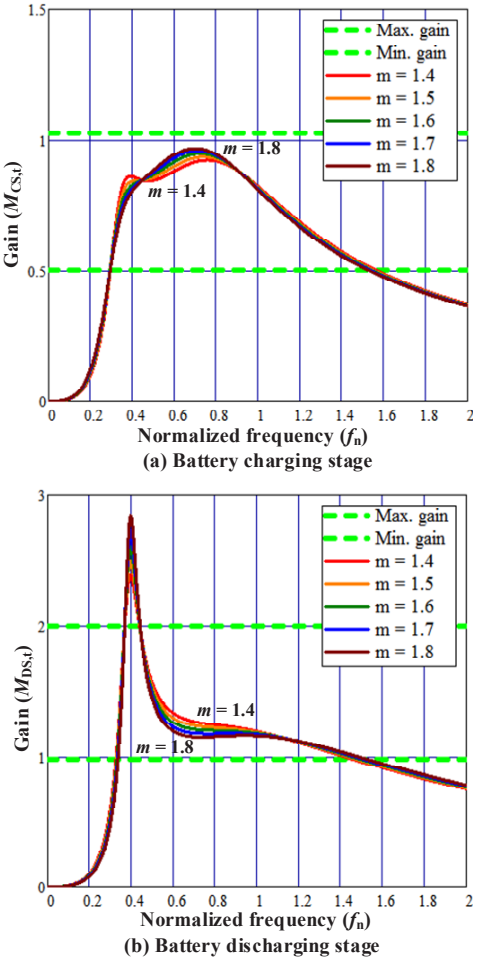

Fig. 8. Voltage-gain curves with different values of m.

IV. Experimental Results

The circuit specifications of 5-kW bidirectional DC-DC CLLLC resonant converter are listed in Table I. This converter is applied between the DC bus and the battery of the electric vehicle to control the bidirectional power flow.

TABLE I. SPECIFICATIONS OF THE BIDIRECTIONAL DC-DC RESONANT CONVERTER

Parameters	Value
DC bus voltage (V_{dc})	400V
Battery voltage (V_{bat})	200~400V
Maximum output current (I_{bat} and I_{dc})	12.5A
Operating frequency (f_s)	48 kHz

A prototype converter of 5-kW bidirectional DC-DC CLLLC resonant converter has been simulated by the simulation software SIMPLIS and implemented in the laboratory to verify the circuit analysis and design. Table II shows the key circuit parameters. Due to the bidirectional symmetric structure of the circuit topology, the practical series resonant frequency in both directions of power flow can be calculated as 90.8 kHz. The varied range of operating frequency in charging stage is about 110 kHz, and the varied range of operating frequency in discharging stage is about 90 kHz.

TABLE II. KEY CIRCUIT PARAMETERS

Parameters	Value
Operating frequency in charging stage ($f_{s,CS}$)	70~180 kHz
Operating frequency in discharging stage ($f_{s,DS}$)	50~140 kHz
Transformer turns-ratio (n)	1.2
Magnetizing inductance (L_m)	54.4 μH
DC bus side resonant inductance (L_{r1})	13.4 μH
Battery side resonant inductance (L_{r2})	9.3 μH
DC bus side resonant capacitance (C_{r1})	204 nF
Battery side resonant capacitance (C_{r2})	340 nF
Filter capacitance (C_{dc} and C_{bat})	60 μF
Switches (S_1–S_8)	IPW65R041CFD (650 V / 68.5 A)

A. Experimental Results and Discussions in Charging Stage

Fig. 9 shows the measured waveforms of v_{r1}, i_{r1}, v_{r2} and i_{r2} under different load conditions at DC bus voltage 400 V and battery voltage 200 V in charging stage. When the output load increases, the operating frequency decreases.

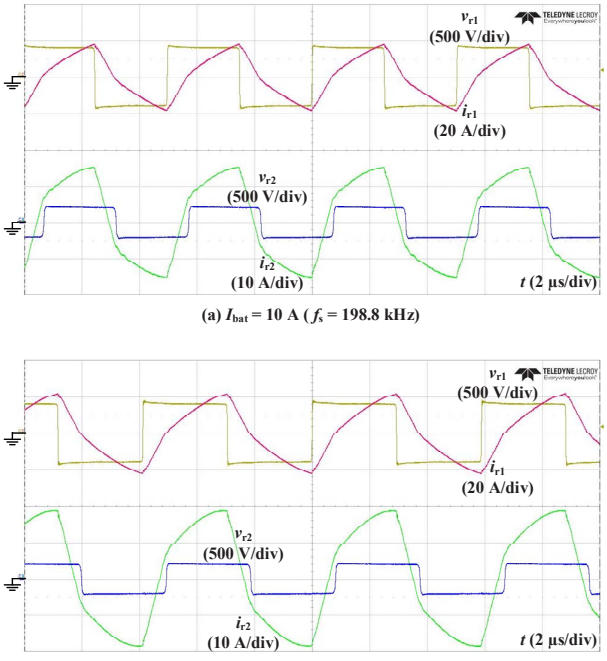

Fig. 9. The waveforms of v_{r1}, i_{r1}, v_{r2} and i_{r2} at V_{dc} = 400 V and V_{bat} = 200 V in CS.

Fig. 10 shows the measured waveforms of v_{r1}, i_{r1}, v_{r2} and i_{r2} under different load conditions at DC bus voltage 400 V and battery voltage 300 V in charging stage. Since the converter is operated in region 1 at these test conditions, that

the circuit characteristics are similar to the SRC converter, nearly 36-kHz frequency variation is needed for the converter to maintain the voltage-gain requirement.

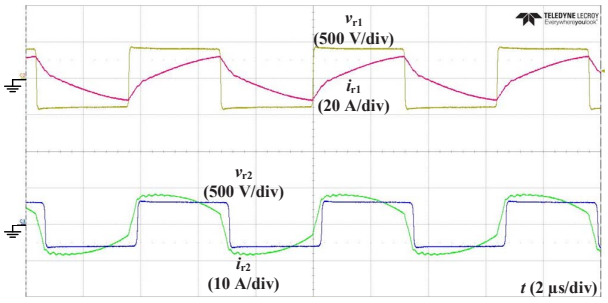

(a) I_{bat} = 6 A (f_s = 156.1 kHz)

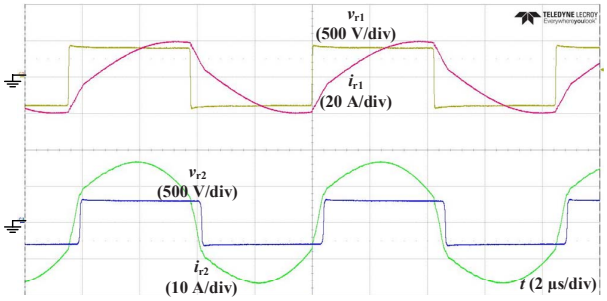

(b) I_{bat} = 12.5 A (f_s = 118.1 kHz)

Fig. 10. The waveforms of v_{r1}, i_{r1}, v_{r2} and i_{r2} at V_{dc} = 400 V and V_{bat} = 300 V in CS.

Fig. 11 shows the measured waveforms of v_{r1}, i_{r1}, v_{r2} and i_{r2} under different load conditions at DC bus voltage 400 V and battery voltage 400 V in charging stage. The circuit characteristics are similar to the LLC converter at these test conditions. Thus, the voltage-gain requirement can be maintained with a small frequency variation. The ringing on v_{r2} is caused by the resonance between the output capacitors of switches and the resonant inductors.

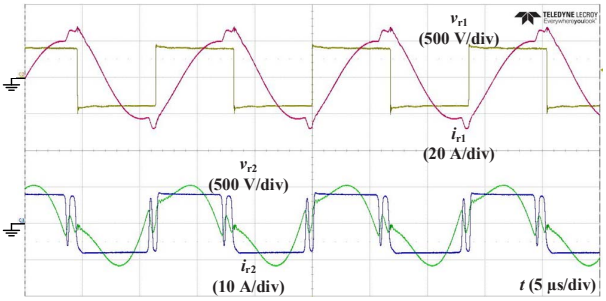

(a) I_{bat} = 6 A (f_s = 73.5 kHz)

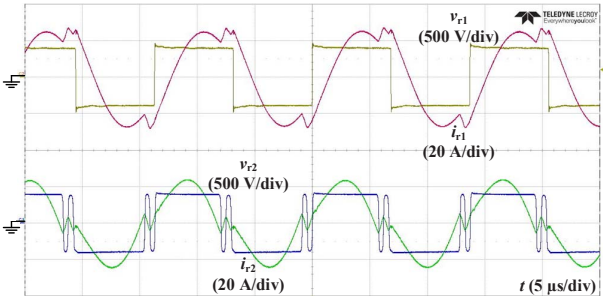

(b) I_{bat} = 12.5 A (f_s = 73.0 kHz)

Fig. 11. The waveforms of v_{r1}, i_{r1}, v_{r2} and i_{r2} at V_{dc} = 400 V and V_{bat} = 400 V in CS.

The efficiency curves at different battery voltage in charging stage are shown in Fig. 12. Since the battery is commonly charged in CC-CV mode, the converter is tested in the lower battery current as the battery voltage increases. The switching loss dominates the power loss at light load conditions, so the efficiency increases when the output current increases. In addition, the test condition of V_{bat} = 300 V has the highest efficiency since the operating frequency is near to the series resonant frequency, and the redundant freewheeling energy can be minimized. The maximum efficiency 96.9% can be achieved in charging stage.

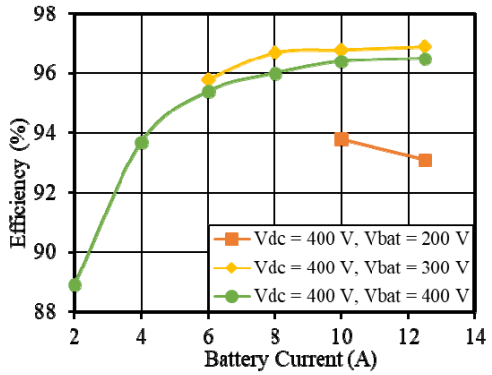

Fig. 12. Efficiency curves at various battery voltage in charging stage.

B. Experimental Results and Discussions in Charging Stage

Fig. 13 shows the measured waveforms of v_{r2}, i_{r2}, v_{r1} and i_{r1} under different load conditions at battery voltage 200 V and DC bus voltage 400 V in discharging stage. After the transformer is decoupled, the ringing on vr1 is caused by the resonance between the output capacitors of switches and the resonant inductors.

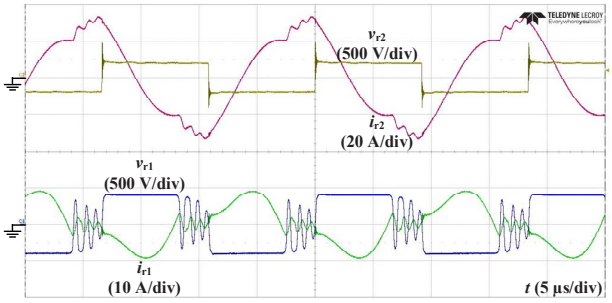

(a) I_{dc} = 4 A (f_s = 54.4 kHz)

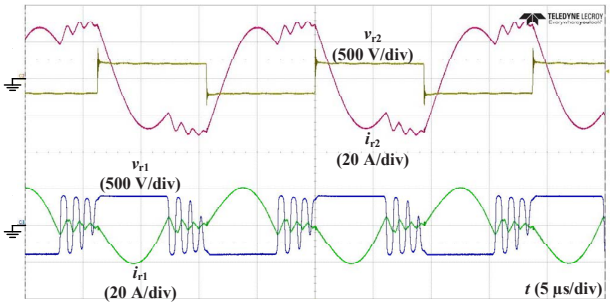

(b) I_{dc} = 8 A (f_s = 53.4 kHz)

Fig. 13. The waveforms of v_{r2}, i_{r2}, v_{r1} and i_{r1} at V_{bat} = 200 V and V_{dc} = 400 V in DS.

Fig. 14 shows the measured waveforms of v_{r2}, i_{r2}, v_{r1} and i_{r1} under different load conditions at battery voltage 300 V and DC bus voltage 400 V in discharging stage. The ringing on v_{r1} is also caused by the resonance between the output capacitors of switches and the resonant inductors. Since the voltage-gain curves are fairly steep at these test conditions, a small frequency variation can make the converter maintain the enough voltage gain.

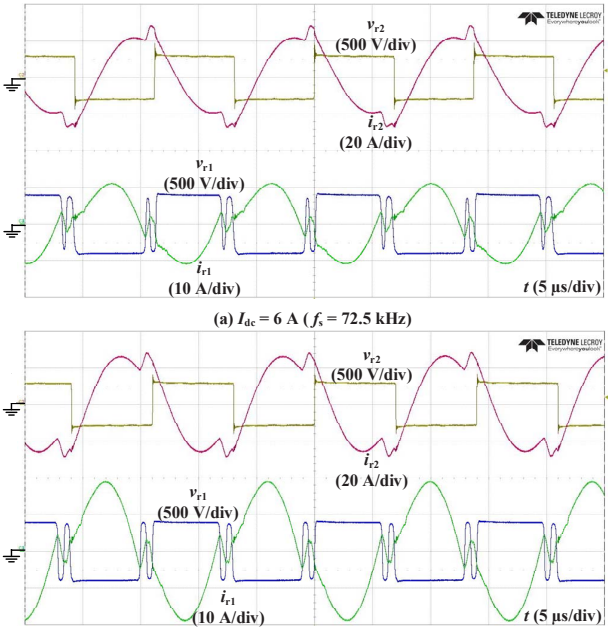

(a) I_{dc} = 6 A (f_s = 72.5 kHz)

(b) I_{dc} = 10 A (f_s = 71.5 kHz)

Fig. 14. The waveforms of v_{r2}, i_{r2}, v_{r1} and i_{r1} at V_{bat} = 300 V and V_{dc} = 400 V in DS.

Fig. 15 shows the measured waveforms of v_{r2}, i_{r2}, v_{r1} and i_{r1} under different load conditions at battery voltage 400 V and DC bus voltage 400 V in discharging stage. The circuit characteristics are similar to the SRC converter at these test conditions, and the parasitic components will make the voltage gain slightly increase at light-load conditions. Therefore, a large frequency variation is needed to maintain the voltage-gain requirement.

The efficiency curves at different battery voltage in discharging stage are shown in Fig. 16. Since the switching loss dominates the power loss at light load conditions, the efficiency increases as the output current increases. However, the conduction loss dominates the power loss at heavy load conditions, so the efficiency decreases when the output current increases further. In addition, the lower battery voltage condition requires a higher current to provide the same power, which will increase the conduction loss. Thus, the higher battery voltage conditions have higher efficiency. The maximum efficiency 97.2% can be achieved in discharging stage.

V. Conclusions and Future Work

According to the comparisons and discussions of the bidirectional topologies, the bidirectional DC-DC full-bridge CLLLC resonant converter with variable frequency control approach is adopted in this thesis. This converter is analyzed and implemented for the high-power energy transferring between the 400 V DC bus and the 200~410 V battery pack,

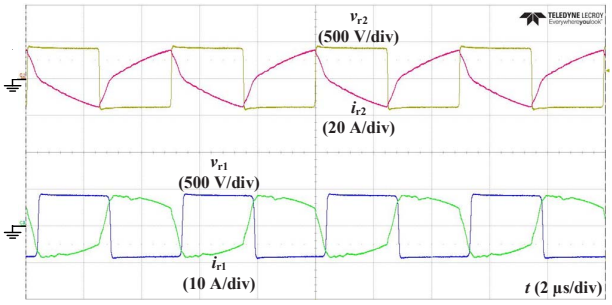

(a) I_{dc} = 6 A (f_s = 198.9 kHz)

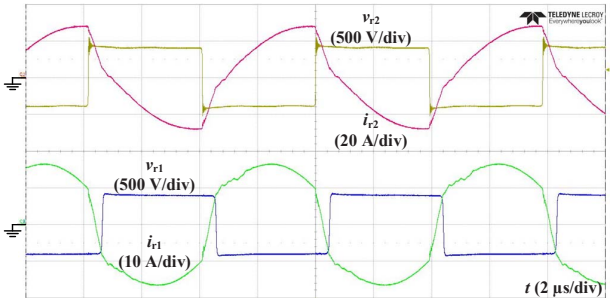

(b) I_{dc} = 12.5 A (f_s = 127.7 kHz)

Fig. 15. The waveforms of v_{r2}, i_{r2}, v_{r1} and i_{r1} at V_{bat} = 400 V and V_{dc} = 400 V in DS.

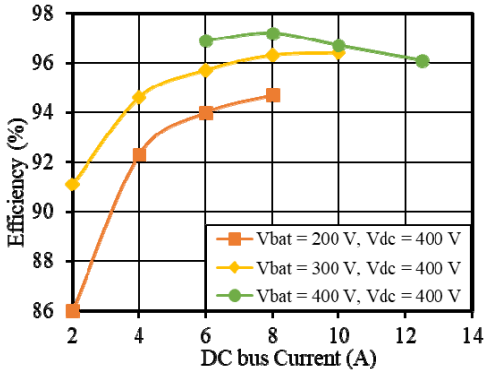

Fig. 16. Efficiency curves at various battery voltage in discharging stage.

which can be applied in the EV chargers and provide galvanic isolation.

The bidirectional resonant converter can be operated under ZVS for the controlled switches and ZCS for the output rectifiers without an additional circuit, which reduces the switching loss and improves the system efficiency. Also, the circuit control is simple because of the symmetrical circuit characteristics of bidirectional power flow. Based on the variable frequency control approach, the steady-state equivalent models of the resonant tank and the voltage-gain characteristics are analyzed. In order to achieve the requirements of voltage gain, the design procedure and the comparisons of voltage-gain curves are discussed in detail. In addition, the power stresses on the circuit components are calculated as well.

A 5-kW laboratory prototype of bidirectional resonant converter is implemented with DSP TMS320F28035. The simulated and experimental results at the different line and load conditions are illustrated to verify the theoretical analysis. The maximum conversion efficiency in charging

stage is 96.9%, and the maximum conversion efficiency in discharging stage is 97.2%.

REFERENCES

[1] M. Yilmaz and P. Krein, "Review of battery charger topologies charging power levels and infrastructure for plug-in electric and hybrid vehicles," IEEE Trans. on Power Electronics, vol. 28, no. 5, pp. 2151-2169, May 2013.

[2] M. Yilmaz and P. T. Krein, "Review of the impact of vehicle-to-grid technologies on distribution systems and utility interfaces," IEEE Trans. on Power Electronics, vol. 28, no. 12, pp. 5673-5689, Dec. 2013.

[3] X. Wang, C. Jiang, B. Lei, H. Bai, and J. L. Kirtley, Jr., "Power-loss analysis and efficiency maximization of a silicon-carbide MOSFET-based three-phase 10-kW bidirectional EV charger using variable-DC-bus control," IEEE Trans. Power Electronics, vol.4, no.3, pp. 880-892, Sep. 2016.

[4] S. Inoue and H. Akagi, "A bidirectional DC-DC converter for an energy storage system with galvanic isolation," IEEE Trans. on Power Electronics, vol. 22, no. 6, pp. 2299-2306, Dec. 2007.

[5] S.Mao, "Isolated bi-directional DC-DC converter with smooth start-up transition," M.S. thesis, Dept. Elect. Eng., Virginia Tech, Blacksburg, VA, May 2015.

[6] H. Fan and H. Li, "High frequency high efficiency bidirectional DC-DC converter module design for 10 kVA solid state transformer," in Proc. IEEE APEC, Feb. 2010, pp. 210-215.

[7] B. Zhao, Q. Yu, and W. Sun, "Extended-phase-shift control of isolated bidirectional DC-DC converter for power distribution in microgrid," IEEE Trans. Power Electron., vol. 27, no. 11, pp. 4667-4680, Nov. 2012.

[8] K. Wang, F. C. Lee, and J. Lai, "Operation principles of bi-directional full-bridge DC-DC converter with unified soft-switching scheme and soft-starting capability," in Proc. IEEE APEC, Feb. 2000, pp. 111-118.

[9] T.-F. Wu, Y.-C. Chen, J.-G. Yang, and C.-L. Kuo, "Isolated bidirectional full-bridge DC-DC converter with a flyback snubber," IEEE Trans. Power Electron., vol. 25, no. 7, pp. 1915-1922, Jul. 2010.

[10] Z. U. Zahid, Z. M. Dalala, R. Chen, B. Chen, and J. S. Lai, "Design of bidirectional DC-DC resonant converter for vehicle-to-grid (V2G) applications," IEEE Trans. Transp. Electrification, vol. 1, no. 3, pp. 232-244, Oct. 2015.

[11] J.-H. Jung, H.-S. Kim, M.-H. Ryu, and J.-W. Baek, "Design methodology of bidirectional CLLC resonant converter for high-frequency isolation of DC distribution systems," IEEE Trans. Power Electron., vol. 28, no. 4, pp. 1741-1755, Apr. 2013.

[12] W. Chen, P. Rong, and Z. Lu, "Snubberless bidirectional DC-DC converter with new CLLC resonant tank featuring minimized switching loss," IEEE Trans. Ind. Electron., vol. 57, no. 9, pp. 3075-3086, Sep. 2010.

[13] T.-T. Wu, "Design and implementation of a bidirectional resonant DC converter," M.S. thesis, Dept. Elect. Eng., National Tsing Hua Univ., Hsinchu, Taiwan, Jul. 2010.

[14] B. Lu, W. Liu, L. Yan, F. C. Lee, and J.D. van Wyk, "Optimal design methodology for LLC resonant converter," in Proc. IEEE APEC, Jun. 2006, pp. 533-538.

[15] J. Hou, "Design procedure for LLC resonant converter," M.S. thesis, Dept. Elect. Eng., National Taiwan Univ., Taipei, Taiwan, Jun. 2009.